

Spectral Density Estimation for Random Fields via Periodic Embeddings

Joseph Guinness

NC State University, Department of Statistics

Abstract

We introduce methods for estimating the spectral density of a random field on a d -dimensional lattice from incomplete gridded data. The methods iteratively impute missing data with periodic conditional simulations on an expanded lattice. Periodic conditional simulations are convenient computationally, in that circulant embedding and preconditioned conjugate gradient methods can produce imputations in $O(n \log n)$ time and $O(n)$ memory. They also have desirable theoretical properties; we prove that both periodogram bias and correlation in the discrete Fourier transform vector can be completely eliminated in some situations, and in general decays faster than $O(n^{-1})$ when the spectral density is sufficiently smooth. In addition, we introduce a filtering method that is designed to reduce periodogram smoothing bias. The methods are demonstrated in numerical and simulation studies, and we present an application to gridded satellite data with missing values. We also describe an implementation of the methods in a publicly available R software package.

1 Introduction

Random fields defined on the integer lattice have wide applications for modeling gridded spatial and spatial-temporal datasets. They also form the basis for some models for non-gridded data (Nychka et al., 2015). The large sizes of modern spatial and spatial-temporal datasets impart an enormous computational burden when using traditional methods for estimating random field models, in particular Gaussian process models. Modeling data on a grid provides a potential solution to the computational issue, since there exist some methods that make use of the fast Fourier transform (FFT). However, there are some pitfalls associated with FFT-based methods related to edge effects and the handling of missing data. This paper provides an accurate and computationally efficient estimation framework for addressing those issues.

Let $Y(x) \in \mathbb{R}$, $x \in \mathbb{Z}^d$ be a mean-zero stationary process on the d -dimensional integer lattice, that is, $E(Y(x)) = 0$ and $\text{Cov}(Y(x), Y(x + h)) = K(h)$ for every x and h in \mathbb{Z}^d . The d -dimensional version of Herglotz's theorem says that the covariance function has a representation in terms of a Fourier transform,

$$K(h) = \int_{[0,1]^d} \exp(2\pi i \omega \cdot h) dF(\omega), \quad (1)$$

where $i = \sqrt{-1}$ and \cdot is the dot product. The function F is a spectral measure, and we assume throughout that it has a continuous derivative f called a spectral density. The focus

here is on estimation of f , which encodes the covariance function, and thus is crucial for prediction of missing values and for regressions when Y is used as a model for residuals. We restrict our attention to stationary models and note that stationary models often form the basis for more flexible nonstationary models that are needed to accurately model many physical processes (Fuentes, 2002).

Suppose that we observe $U = (Y(x_1), \dots, Y(x_n))$ at a distinct set of n locations $\mathbb{S}_1 = \{x_1, \dots, x_n\}$. If f or K have known parametric forms, then we can use likelihood-based methods for estimating the parameters. Evaluating the Gaussian likelihood involves computing, storing, and factoring the covariance matrix for U , which requires $O(n^2)$ memory and $O(n^3)$ floating point operations (FLOPs) if the covariance matrix does not have any exploitable structure. If the locations form a complete rectangular subset of the integer lattice, Whittle's likelihood approximation (Whittle, 1954) can be used, which replaces the nested block Toeplitz covariance matrix with a nested block circulant matrix. Circulant matrices are diagonalized by the discrete Fourier transform (DFT) matrix, and thus FFT algorithms can be employed in order to approximate the likelihood in $O(n \log n)$ flops and $O(n)$ memory. Guyon (1982) showed that the resulting maximum approximate likelihood parameter estimates are not \sqrt{n} consistent when the dimension d of the field is greater than 1. Dahlhaus and Künsch (1987) suggested the use of data tapers to reduce edge effects and proved that the tapered version of the likelihood approximation is asymptotically efficient when $d \leq 3$. Stroud et al. (2017) and Guinness and Fuentes (2017) suggested the use of periodic embeddings and demonstrated their accuracy in numerical studies. Sykulski et al. (2016) introduced a de-biased Whittle likelihood, which can be viewed as a composite likelihood.

If one is not willing to assume that f or K have known parametric forms, and if the data are observed on a complete rectangular grid, nonparametric methods can be used to estimate f . The standard approach is to compute the discrete Fourier transform (DFT),

$$J(\omega) = \frac{1}{\sqrt{n}} \sum_x Y(x) \exp(-2\pi i \omega \cdot x), \quad (2)$$

and estimate of the spectrum with a smoothed version of the periodogram $|J(\omega)|^2$,

$$\hat{f}(\omega) = \sum_{\nu} |J(\nu)|^2 \alpha(\omega - \nu),$$

where α is a smoothing kernel. Selection of the bandwidth of the smoothing kernel has been studied by several authors (Lee, 1997; Ombao et al., 2001; Lee, 2001). Dahlhaus and Künsch (1987) proposed replacing $Y(x)$ in (2) with $Y(x)T(x)$ (and an appropriate scaling), where $T(x)$ is a taper function that tends to zero on the boundary of the observation domain. Alternatively, one can smooth the periodogram through a penalized likelihood approach (Wahba, 1980; Chow and Grenander, 1985; Pawitan and O'Sullivan, 1994) or use a Bayesian approach with smooth priors (Zheng et al., 2009). Politis and Romano (1995) provided a method for reducing bias in the smoothed periodogram. Heyde and Gay (1993) studied asymptotic statistical properties of the periodogram in an increasing domain setting, while Stein (1995) studied them in an increasing resolution setting, noting the importance of filtering the data. Lim and Stein (2008) considered the multivariate case.

All of the methods discussed above apply when a complete dataset is available on a rectangular grid. However, even when available on a grid, spatial datasets often have many missing values; for example, it is common to encounter gridded satellite datasets with some values obscured by clouds. Missing values complicate two aspects of periodogram-based estimators. The first is that a surrogate for the missing values must be substituted; Fuentes (2007) suggested replacing them with zeros. A second problem is that scattered missing values seriously disrupt the use of differencing filters. For example two-dimensional differencing at observed location (j, k) can be applied only if observations at $(j + 1, k)$, $(j, k + 1)$, and $(j + 1, k + 1)$ are observed as well.

To address these issues, this paper introduces computationally efficient methodology for estimating the spectrum based on imputing missing values with conditional simulations and iteratively updating the spectrum estimate, in a similar vein as Lee and Zhu (2009) proposed for time series data. The novelty of our approach is that the missing values are imputed in a periodic fashion on an expanded lattice. Periodic imputations are convenient computationally, since circulant embedding and preconditioned conjugate gradient methods can be used for solving the linear systems required for imputation in $O(n \log n)$ time and $O(n)$ memory. Periodic imputation has desirable theoretical properties as well; we prove that it completely eliminates periodogram bias and correlation in the discrete Fourier transform vector in certain situations. In more general situations, periodic imputation gives bias and correlation decay rates that are faster than $O(n^{-1})$ when the spectrum is sufficiently smooth. We also provide theoretical results describing when the imputed data spectrum is expected to give an estimate with a smaller bias than the spectrum used for imputation, which suggests that any existing spectral density estimate can be improved through periodic imputation.

The theoretical results provide a sound basis for the nonparametric estimation methods and give some insight into why the parametric methods in Guinness and Fuentes (2017) perform so well in simulations. Additionally, this paper introduces a parametric filtering method based on fitting simple parametric models within the iterative method. The fitted parametric models can be used to filter the data, which is effective for reducing bias due to periodogram smoothing. Taken together, this work results in accurate and computationally efficient methods for estimating spectral densities when the gridded data have arbitrary missingness patterns. We provide thorough numerical and simulation studies for the methods and demonstrate that even a small amount of lattice expansion provides substantial bias and correlation reduction. We apply the methods to an incomplete land surface temperature dataset, and we also describe a publicly available R software package implementing the methods.

2 Methodology

2.1 Notation and Background

Let $y = (y_1, \dots, y_d)$ with $y_i \in \mathbb{N}$, and define the hyperrectangle $\mathbb{J}_y \subset \mathbb{Z}^d$, where

$$\mathbb{J}_y = \{(a_1, \dots, a_d) | 1 \leq a_j \leq y_j \ \forall j\}.$$

If $d = 2$, this is simply a rectangular lattice of size (y_1, y_2) . We assume that the observation locations \mathbb{S}_1 form a subset \mathbb{J}_y , and so we call \mathbb{J}_y the observation lattice. Define V to be the

vector containing the process at the remaining locations $\mathbb{J}_y \setminus \mathbb{S}_1$.

Let f_k be a spectral density and E_k denote expectation in the mean zero multivariate normal distribution for (U, V) under f_k with covariance given by (1). For time series data, Lee and Zhu (2009) proposed an iterative method for obtaining nonparametric estimates of the spectrum. Their method can be extended from one dimension to general dimensions as follows. Define f_{k+1} as

$$f_{k+1}(\omega) = \sum_{\nu \in \mathbb{F}_y} E_k \left(|J(\nu)|^2 \mid U \right) \alpha(\omega - \nu),$$

where \mathbb{F}_y is the set of Fourier frequencies associated with a grid of size y . Here, we use a smoothing kernel, but Lee and Zhu (2009) noted that any smoothing method can be applied. The conditional expectation of the periodogram under f_k is computationally expensive, so Lee and Zhu (2009) proposed replacing the expected value with an average over L independent realizations of V given U , as in

$$f_{k+1}(\omega) = \sum_{\nu \in \mathbb{F}_y} \frac{1}{L} \left(\sum_{\ell=1}^L |J^{(\ell)}(\nu)|^2 \right) \alpha(\omega - \nu),$$

where $J^{(\ell)}$ is the periodogram derived from $(U, V^{(\ell)})$, where $V^{(1)}, \dots, V^{(L)}$ are independent conditional simulations of V given U under f_k . The procedure is then iterated over k until convergence. Replacing the conditional expectation with a sample average is analogous to the approach taken in the iterative method in Tanner and Wong (1987) for Bayesian estimation of parametric statistical models.

2.2 Periodic Imputation

When $d > 1$, edge effects become a prominent issue (Guyon, 1982); in particular, the Whittle likelihood can be interpreted as the exact likelihood for a model in which the field is periodic on the observation lattice (Guinness and Fuentes, 2017). Data tapers have been proposed to alleviate the issue, but tapering can lead to loss of information from data near the boundaries or near missing values. In this paper, we propose extending the hyperrectangle in each dimension and performing the imputations under a periodic approximation to the covariance function. Surprisingly, using the periodic approximation to the covariance function for the imputations, rather than the true covariance function, leads to improved spectral density estimates. Periodic models also allow for the use of circulant embedding techniques to draw from V given U efficiently.

Let $\tau \geq 1$, and define $z_j = \lceil \tau y_j \rceil$ so that $z_j \geq y_j$ for $j = 1, \dots, d$. Define $m = z_1 \cdots z_d$ to be the total number of locations in \mathbb{J}_z , which we refer to as the embedding lattice. Let f_k be a spectral density and R_k be the covariance function

$$R_k(h) = \frac{1}{m} \sum_{\omega \in \mathbb{F}_z} f_k(\omega) \exp(2\pi i \omega \cdot h). \quad (3)$$

where \mathbb{F}_z are the Fourier frequencies associated with \mathbb{J}_z . Note that R_k is periodic on \mathbb{J}_z and is not the integral Fourier transform of f_k that appears in (1). Let V denote the vector of

missing values on $\mathbb{J}_z \setminus \mathbb{S}_1$ and \tilde{E}_k denote expectation in the mean-zero multivariate normal distribution for (U, V) with covariance function $R_k(\cdot)$. Define f_{k+1} as

$$f_{k+1}(\omega) = \sum_{\nu \in \mathbb{F}_z} \tilde{E}_k \left(|J(\nu)|^2 | U \right) \alpha(\omega - \nu).$$

Note that the conditional expectation in the Lee and Zhu (2009) estimator is done on the observation lattice and using the correct model, whereas here, we use the conditional expectation under a model that is periodic on the embedding lattice.

To see how the conditional simulations of V given U can be computed efficiently, define R_k to be the covariance matrix for (U, V) under covariance function $R_k(\cdot)$, and partition it as

$$R_k = \begin{bmatrix} A_k & B_k \\ B_k^T & C_k \end{bmatrix},$$

where A_k and C_k are the covariance matrices for the observations U and missing values V , respectively. The conditional expectation for V given U is $\tilde{E}_k(V|U) = B_k^T A_k^{-1} U$. The most demanding computational step for obtaining $\tilde{E}_k(V|U)$ is solving the linear system $A_k x = U$. Preconditioned conjugate gradient methods for solving linear systems (Greenbaum, 1997) are efficient when the forward multiplication $A_k x$ can be computed efficiently, and when we can find a matrix M , called the preconditioner, for which $MA_k \approx I$ and for which Mx can be computed efficiently as well. In the present situation, multiplying A_k by x can be done via the embedded multiplication

$$R_k \begin{bmatrix} x \\ 0 \end{bmatrix} = \begin{bmatrix} A_k & B_k \\ B_k^T & C_k \end{bmatrix} \begin{bmatrix} x \\ 0 \end{bmatrix} = \begin{bmatrix} A_k x \\ B_k^T x \end{bmatrix}.$$

This embedded multiplication can be done in $O(m \log m)$ time because matrix-vector multiplications with R_k can be computed at the cost of two fast Fourier transforms (FFTs).

There exist various preconditioning methods. For example, one can use $M = (A_k - B_k C_k^{-1} B_k^T)^{-1}$, since that is a submatrix of R_k^{-1} , and FFTs can be used to do matrix multiplications with R_k^{-1} . We have found that a preconditioning method based on the Gaussian likelihood approximation due to Vecchia (1988) works particularly well. Stroud et al. (2017) proposed Vecchia's approximation as a preconditioner but favored the use of R_k^{-1} , citing slow running times. A recent implementation of Vecchia's approximation in a low-level computing language have improved the running times, and have now made it a viable competitor as a preconditioner. Section 5 includes some timing comparisons.

The imputation method requires not just a conditional expectation but a conditional simulation of V given U . It is well-known that conditional simulations can be computed at the cost of one unconditional simulation and two conditional expectations (Chiles and Delfiner, 2009). Circulant embeddings again are used for unconditional simulation of (U, V) under covariance R_k at the cost of two FFTs. See Wood and Chan (1994) or Guinness and Fuentes (2017) for details.

2.3 Variant with parametric filter

Even if $|J(\omega)|^2$ is unbiased for $f(\omega)$, the smoothing step can introduce some bias in the spectral density estimate if the spectral density is not nearly linear around ω . For spectral

densities with large dynamic range, data filters have been proposed to pre-whiten the data prior to smoothing (Stein, 1995). Missing data pose a challenge for data filters, but filters can be easily applied to the imputed data at each iteration. In this subsection, we propose a parametric filtering method that we show is successful in reducing smoothing bias.

Let f_θ be a parametric spectral density. The imputed data Whittle likelihood approximation is defined as

$$\ell(\theta) = -\frac{m}{2} \log 2\pi - \frac{1}{2} \sum_{\omega \in \mathbb{F}_z} \left(\log f_\theta(\omega) + \frac{\tilde{E}_k(|J(\omega)|^2 | U)}{f_\theta(\omega)} \right).$$

Let θ_k be the maximizer of $\ell(\theta)$. Then define

$$f_{k+1}(\omega) = f_{\theta_k}(\omega) \sum_{\nu \in \mathbb{F}_z} \frac{\tilde{E}_k(|J(\nu)|^2 | U)}{f_{\theta_k}(\nu)} \alpha(\omega - \nu).$$

As before, in practice we replace $\tilde{E}_k(|J(\nu)|^2 | U)$ with a sample average that can be computed efficiently. The completely nonparametric variant is a special case with $f_\theta(\omega)$ constant. Using the parametric step in the smoothing serves to flatten the periodogram, which we show in simulation studies is helpful for reducing smoothing bias. This allows for the use of wider smoothing kernels, which reduces variance as well.

3 Theory

We use the notation that f is the true spectrum and that R (without parentheses), partitioned as $[A \ B; B^T \ C]$, is the block circulant covariance matrix for (U, V) under periodic covariance function $R(\cdot)$ derived from spectrum f on embedding lattice \mathbb{J}_z . Let K denote the covariance matrix for U under the true nonperiodic covariance function $K(\cdot)$ in (1). Note that R is $m \times m$, while K is $n \times n$. Let f_1 be a spectrum to be used for imputation, which we refer to as the imputation spectrum. Define R_1 (derived from f_1), A_1 , B_1 , and C_1 accordingly. Throughout, we assume that both f and f_1 are bounded above and below by positive constants. If V_1 is a periodic conditional simulation given observations U under f_1 , then the true covariance matrix for (U, V_1) is

$$S := \text{Cov} \left(\begin{bmatrix} U \\ V_1 \end{bmatrix} \right) = \begin{bmatrix} K & KA_1^{-1}B_1 \\ B_1^T A_1^{-1}K & C_1 - B_1^T A_1^{-1}B_1 + B_1^T A_1^{-1}KA_1^{-1}B_1 \end{bmatrix}.$$

Define the $m \times 1$ vector $g(\nu)$ to have entries $m^{-1/2} \exp(2\pi i \nu \cdot x)$, where $\nu \in \mathbb{F}_z$ is a Fourier frequency, and $x \in \mathbb{J}_z$, with the entries of $g(\nu)$ ordered as they are in (U, V) . Define

$$\tilde{f}_1(\nu, \omega) := E(\tilde{E}_1(J(\nu)J(\omega)^* | U)) = g(\nu)^\dagger S g(\omega),$$

where $*$ is complex conjugate, and \dagger is conjugate transpose, so that $\tilde{f}_1(\nu, \nu)$ is the Fourier spectrum of S from which we construct our estimates of the spectrum. Likewise, we define $f(\nu, \omega) = f(\nu)$ if $\omega = \nu$ and 0 if $\omega \neq \nu$. This notation is useful for succinct theorem statements and reflects the fact that the true bispectrum is zero off the diagonal for stationary

models. It is of interest to study $\tilde{f}_1(\nu, \omega) - f(\nu, \omega)$, which for $\omega = \nu$ corresponds to the bias of the periodogram, and for $\omega \neq \nu$ measures dependence in the periodogram, both of which should ideally be near zero.

The first result establishes that when the covariance function is compactly supported, the imputation spectrum is correct, and the imputation lattice \mathbb{J}_z is chosen to be large enough, then the imputed periodogram is exactly unbiased, and the bispectrum is exactly zero. This is in contrast to the usual non-imputation results on periodograms, which typically have a bias of order $n^{-1/d}$ (Guyon, 1982), which can be reduced to order n^{-1} with data tapers (Dahlhaus and Künsch, 1987) but come with a variance tradeoff. All proofs are found in Appendix A

Theorem 1. *If $f_1 = f$, $K(h) = 0$ for all $\|h\| > h_0$, and $|z_j - y_j| > h_0$ for all $j \in \{1, \dots, d\}$, then for every $\nu, \omega \in \mathbb{F}_z$,*

$$\tilde{f}(\nu, \omega) - f(\nu, \omega) = 0.$$

The next result is more general in that we only require K to decay at a certain rate, which is equivalent to placing smoothness conditions on the spectrum. The tradeoff is that we obtain non-zero bounds on $\tilde{f}_1(\nu, \omega) - f(\nu, \omega)$, but the rates are better than the usual $n^{-1/d}$ or even n^{-1} rates for the bias of the non-imputed periodograms when the spectrum is smooth enough. The assumptions about how the observation grid grows with n are standard assumptions that ensure that each dimension grows at the same rate with n .

Theorem 2. *If f has p continuous partial derivatives, $f_1 = f$, $y_j = O(n^{1/d})$, and $z_j = O(\tau y_j)$ for $\tau > 1$, then for every $\nu, \omega \in \mathbb{F}_z$,*

$$\tilde{f}_1(\nu, \omega) - f(\nu, \omega) = O(n^{-p/d+1}).$$

The previous theorems all assumed that the imputation spectrum was correct. The following theorem relaxes this assumption and gives bias rates in terms of the difference between the true spectrum and the imputation spectrum. The implication of the theorem is that, when the conditions are satisfied, we can take f_1 to be any estimate of the spectrum, and the bias of \tilde{f}_1 is smaller than the bias of f_1 , that is, any estimate can be improved by periodic imputation.

Theorem 3. *Let f have p continuous partial derivatives, and assume the same conditions on the observation and embedding lattice as in Theorem 2. Define $\Delta_1 = \max_{\omega \in \mathbb{T}^d} |f(\omega) - f_1(\omega)|$. Then for every $\nu, \omega \in \mathbb{F}_z$,*

$$\tilde{f}_1(\nu, \omega) - f(\nu, \omega) = O(n^{-p/d+1}) + O\left(\Delta_1 \sqrt{\frac{m-n}{m}}\right),$$

meaning that the difference contains two terms with the respective rates.

4 Numerical Studies and Simulations

To provide more insight about the behavior of the proposed estimation methods, we present numerical studies analyzing the bispectrum of the imputed data and simulation results comparing the proposed methods to standard spectral density estimators. In the first numerical

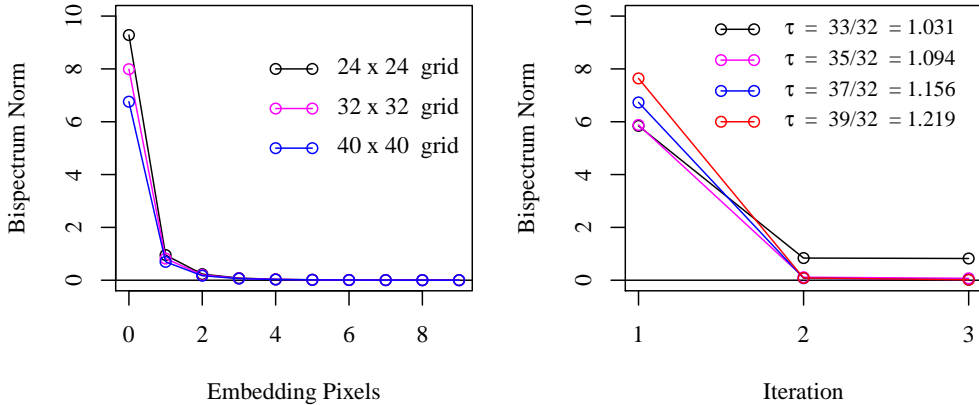


Figure 1: Normalized squared bispectrum error for imputation with correct spectrum (left) and iteratively updating the imputation spectrum on a 32×32 grid (right).

study, we assume that the true covariance function is $K(h) = 2 \exp(-\|h\|/8)$, and we observe complete datasets on grids of size $(24, 24)$, $(32, 32)$, and $(40, 40)$. We compute the bispectrum of S with f_1 equal to the true spectrum for several embedding sizes, including an option of zero embedding (i.e. $z = y$ or $\tau = 1$). We quantify the error in the bispectrum with an integrated normalized squared bias

$$\frac{1}{m} \sum_{\nu \in \mathbb{F}_z} \sum_{\omega \in \mathbb{F}_z} \frac{\left(\tilde{f}_1(\nu, \omega) - f(\nu, \omega) \right)^2}{f(\nu, \nu) f(\omega, \omega)}.$$

The results for the first numerical study are in the left panel of Figure 1. When no embedding is used, the bispectrum has a substantial bias, but the bias quickly decays towards zero as the embedding size increases. Remarkably, the integrated normalized squared bias is essentially zero after only 4 embedding pixels, even though the exponential correlation range is twice that distance.

The second numerical study considers convergence of the iterative procedure. Consider the same covariance function as before and fix the grid size at $(32, 32)$. Define f_1 as the bispectrum of K ,

$$f_1(\nu, \omega) = \frac{m}{n} g(\nu)^\dagger \begin{bmatrix} K & 0 \\ 0 & 0 \end{bmatrix} g(\omega).$$

Then for $k \geq 1$, define f_{k+1} to be $g(\nu)^\dagger S_k g(\omega)$, where

$$S_k = \begin{bmatrix} K & K A_k^{-1} B_k \\ B_k^T A_k^{-1} K & C_k + B_k^T A_k^{-1} (K - A_k) A_k^{-1} B_k \end{bmatrix}.$$

This numerical study mirrors a setting where we initialize the iterative procedure with the periodogram of the non-imputed data. The results for the integrated normalized squared bias are plotted in the right panel of Figure 1. The iterative procedure converges remarkably fast for the various choices of τ . There is essentially no difference between f_2 and f_3 . The

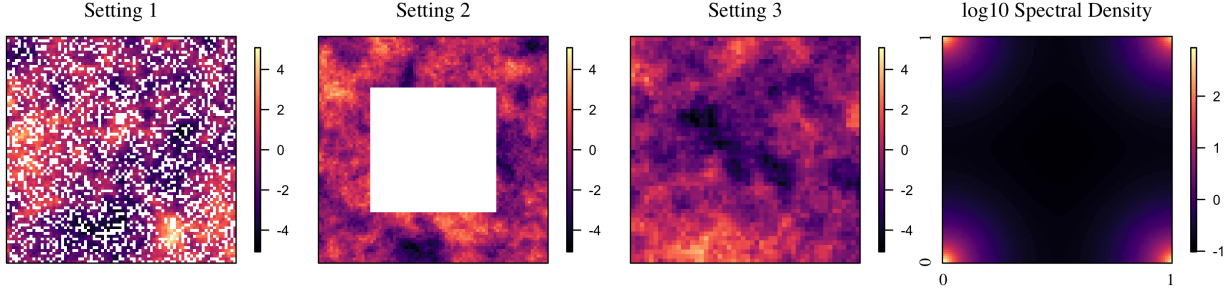


Figure 2: Example realizations from the three simulation settings, with missing values in white. Rightmost plot is the assumed log spectral density.

accuracy also increases with the size of the embedding lattice, with τ as small as 1.1 giving accurate results.

The first simulation setting has an 80×80 grid with 30% of the observations missing at random. The second has an 80×80 grid with a square of missing values in the center, covering roughly 30% of the grid area. The third setting has no missing values but a smaller grid of size 50×50 . Settings 1 and 2 are designed to show situations in which traditional spectral methods may fail, while Setting 3 shows a setting in which traditional methods should perform well. Data in all settings are generated from a Gaussian process model with mean 0, assumed to be known, and exponential covariance function $K(h) = 2 \exp(-\|h\|/8)$. Example datasets from each of these settings are given in Figure 2

We consider several methods for estimating the spectral densities. The first method was suggested by Fuentes (2007). Define $Y^0(x)$ to equal $Y(x)$ if data is available at location x and 0 otherwise. Then define the discrete Fourier transform

$$J^0(\omega) = \frac{1}{\sqrt{n}} \sum_{x \in \mathbb{J}_y} Y^0(x) \exp(-2\pi i \omega \cdot x),$$

where n is the number of non-missing values. The spectral density estimate is then a smoothed version of the zero-imputed periodogram.

The second method uses a periodogram computed from tapered data, as described in the Introduction. We define one-dimensional cosine tapers T_1 and T_2 applied to 5% of the observations on each of the two edges, and the taper function is the outer product $T((j, k)) = T_1(j)T_2(k)$. The spectral density estimate is then a smoothed version of the tapered periodogram, normalized by the sum of the squared taper function. In Setting 2, which includes a square of missing values in the center, we also taper the interior observations, as indicated in Figure 3. In Settings 1 and 3, we taper only the exterior observations.

For the imputation-based methods proposed in this paper, we consider lattice expansion factors $\tau \in \{1.0, 1.1, 1.2, 1.3\}$. We also consider two settings for the use of a parametric filter, the first being no filter, and the second with a filter of the form

$$f_\theta(\omega) = \frac{1}{1 - \frac{\theta}{2}(\cos(2\pi\omega_1) + \cos(2\pi\omega_2))}, \quad (4)$$

where $-1 < \theta < 1$. This choice for the parametric model is deliberately misspecified with respect to the true form of the data-generating spectrum. Lindgren et al. (2011) showed that

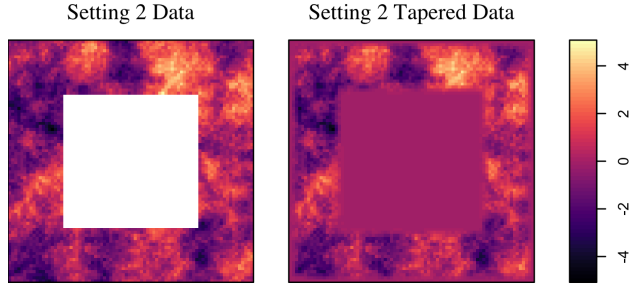


Figure 3: Original and interior/exterior tapered data from Setting 2.

this model can approximate the Matérn covariance with smoothness parameter equal to 1, whereas the true model is exponential, which corresponds to Matérn with smoothness 1/2.

All of the periodic embedding estimation methods use $L = 1$ conditional simulation per iteration and are run for 200 iterations. The estimate from the k th dataset is denoted by \hat{f}_k and is obtained by averaging the spectra over the last 100 iterations. All methods use a Gaussian smoothing kernel proportional to $\exp(-\|\omega - \nu\|^2/\delta^2)$, where the distance $\|\omega - \nu\|$ is defined periodically on the domain $[0, 1]^2$. We consider two metrics for evaluating the estimation methods. The first is a relative bias

$$\text{BIAS}(\omega) = \frac{1}{K} \sum_{k=1}^K \frac{\hat{f}_k(\omega) - f(\omega)}{f(\omega)},$$

where $K = 100$ is the total number of simulated datasets, and f is the true spectrum. The second metric is a mean relative squared error (MSE)

$$\text{MSE}(\omega) = \frac{1}{K} \sum_{k=1}^K \left(\frac{\hat{f}_k(\omega) - f(\omega)}{f(\omega)} \right)^2.$$

To evaluate relative bias on an equal footing, we compare all methods using a small value of $\delta = 0.02$. Figure 4 contains plots of the relative bias for the non-tapered and tapered methods, and non-filtered and filtered periodic embedding methods with $\tau = 1.2$. In Setting 1, the non-tapered and tapered methods have a very large relative bias at almost every frequency. They estimate far too much power at higher frequencies, due to the fact that imputing with zeros produces fields that are rougher than the underlying process. In contrast, the periodic embedding methods have very small bias. In Setting 2, the non-tapered and tapered biases improve, but are still larger than the periodic embedding biases, especially for low frequencies. The relative biases for non-tapered and tapered methods are similar in Setting 3 and are still larger than the periodic embedding relative biases. Though not shown here, the biases for $\tau = 1.1$ and 1.3 are similar. The parametric filters serve to reduce the bias compared to not filtering. The periodic embedding methods have a small bias near $\omega = (0, 0)$; based on the accuracies shown in the numerical studies, this bias is likely due to smoothing bias because of the sharply-peaked spectra near the origin.

To evaluate mean relative squared error on an equal footing, all methods were computed with a range of choices for δ ; the reported results are for the value of δ that minimized the

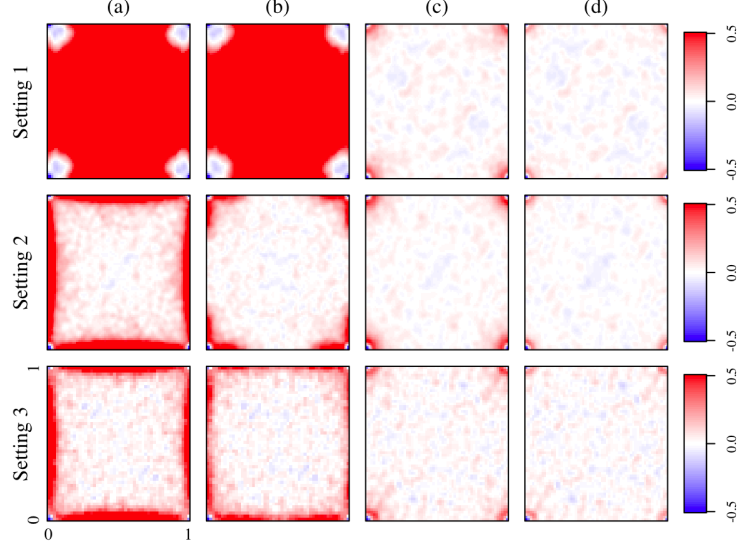


Figure 4: Relative bias as a function of frequency for the three simulation settings, and the four estimation settings: (a) not tapered, (b) tapered, (c) $\tau = 1.2$, no filter, (d) $\tau = 1.2$, parametric filter.

root integrated MSE (RIMSE)

$$\text{RIMSE} = \sqrt{\frac{1}{m} \sum_{\omega \in \mathbb{F}_z} \text{MSE}(\omega)},$$

the square root of the average MSE over all Fourier frequencies.

Table 4 contains RIMSE results for the various methods. The periodic embedding methods with $\tau > 1$ are more accurate than both the non-tapered and tapered periodogram estimates in every case. In Setting 1, the non-tapered and tapered estimates are quite poor, likely due to the large biases seen in Figure 4. For periodic embedding, we see that the RIMSE values improve when $\tau > 1$ but do not improve beyond $\tau = 1.1$. This is consistent with the numerical studies that showed a small amount of periodic embedding was sufficient. Filtering provides a further improvement, reducing RIMSE by 30-40%. In Setting 2, the non-tapered and tapered estimates improve substantially, and the periodic embedding methods offer further improvement. One thing to note from Settings 1 and 2 is that imputing alone is not sufficient; one really needs to do the imputations in a periodic fashion on an expanded lattice. This can be seen by comparing the $\tau = 1.0$ results to the $\tau > 1$ results. In Setting 3, the parametric filter performs similarly to tapering, but periodic embedding with parametric filtering is by far the most accurate method when $\tau > 1$.

The methods developed in this paper show large improvements in Settings 1 and 2, where we do not expect traditional nonparametric spectral methods to perform well. The results for Setting 3 indicate that the periodic embedding and parametric filter methods are capable of offering large improvements over traditional nonparametric spectral methods even in a case where we expect traditional methods to perform well.

Estimation Settings		Simulation Setting		
		1	2	3
No Impute	No Taper	3.2830	0.5172	0.4836
No Impute	Taper	3.2226	0.2871	0.3324
$\tau = 1.0$	No Filter	0.3030	0.4023	0.4836
$\tau = 1.0$	Filter	0.2408	0.2950	0.3517
$\tau = 1.1$	No Filter	0.2042	0.2182	0.2693
$\tau = 1.1$	Filter	0.1373	0.1351	0.1587
$\tau = 1.2$	No Filter	0.2060	0.2190	0.2615
$\tau = 1.2$	Filter	0.1366	0.1325	0.1553
$\tau = 1.3$	No Filter	0.2101	0.2208	0.2646
$\tau = 1.3$	Filter	0.1362	0.1316	0.1559

Table 1: Integrated relative MSE results

5 Software and Application to Satellite Data

The methods are implemented in an R package titled “npspec” and made freely available through the author’s public github page <https://github.com/joeguinness/npspec>. The main function for estimating the spectrum is `iterate_spec`, which takes the following arguments: `y`, a matrix of data values; `observed`, a logical-valued matrix of the same size as `y`, with TRUE entries indicating non-missing values, and FALSE entries indicating missing values; `embed_fac`, which is the embedding factor τ ; `burn_iters`, the number of burn-in iterations (described below); `par_spec_fun`, which currently takes values `spec_AR1`, indicating that the function should filter using the spectrum in (4), or `FALSE`, indicating that no parametric filtering should be used; `kern_parm`, the kernel smoothing parameter δ ; `precond_method`, either “`fft`” for the inverse spectrum preconditioner or “`Vecchia`” for the Vecchia preconditioner; and `m`, the number of neighbors when the Vecchia preconditioner is used. In addition to returning an estimated spectrum `spec`, `iterate_spec` returns a conditional expectation map filling in the missing values, a conditional simulation map, and a Vecchia approximation to the likelihood.

Additionally, there is a function `condexp` for computing predictions at the locations of the missing values. It has arguments `y`, `observed`, and `spec`, the spectrum to be used for prediction. There is also a function `condsim` for computing L conditional simulations given data `y`, observation locations `observed`, and a spectrum `spec`.

To illustrate the practical usefulness of the proposed methods, we analyze a gridded land surface temperature dataset. These data were used recently in Heaton et al. (2017). The data were originally collected by the Moderate Resolution Imaging Spectrometer (MODIS) on board the NASA Terra Satellite. The region is a grid of 500 by 300 locations in the latitudinal range of 34.295 to 37.068 and longitudinal range of -95.912 to -91.284 , giving a grid spacing of just under 0.01 degrees in both latitude and longitude, which translates to roughly 1100 m in the north/south dimension, and 900m in the east/west dimension. The total size of the region is roughly 450 km by 300 km, covering parts of the US states of Oklahoma, Arkansas, Kansas, and Missouri. The values in the dataset represent land surface temperature in degrees Celsius. They were collected on a summer day, August 4,

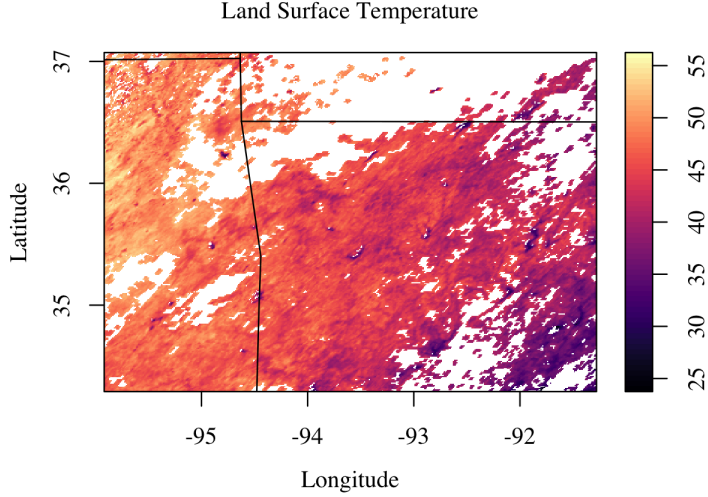


Figure 5: Surface temperature dataset in degrees Celsius. State boundaries in black.

2016, and 7 percent of the land surface temperatures are larger than 50 Celsius. The dataset has 105,569 non-missing values, which are plotted in Figure 5. We can see that there is a distinct trend from the southeast to the northwest corner, so we use least squares to fit a linear trend in latitude and longitude and apply the spectrum estimation methods to the residuals.

The choice of L , the number of imputations per iteration, need not be held constant during the iterative procedure. We have found, similarly to Tanner and Wong (1987), that L also need not be very large; in fact, we have achieved good results with $L = 1$. We then use successive iterations to form averages. Formally, our alternative method is to choose B , a number of burn-in iterations, and run the iterative procedure with $L = 1$ until we obtain f_B . At each successive iteration, we simulate $V^{(B+k)}$ from the conditional distribution for V given U under the spectrum \bar{f}_{B+k} , compute the periodogram $|J^{(B+k)}(\nu)|^2$, and update the spectrum as

$$\bar{f}_{B+k+1}(\omega) = \frac{k}{k+1} \bar{f}_{B+k}(\omega) + \frac{1}{k+1} \sum_{\nu \in \mathbb{F}_z} |J^{(B+k)}(\nu)|^2 \alpha(\omega - \nu),$$

a weighted averaged of the previous spectrum and the current smoothed periodogram. Convergence is determined by the criterion

$$\max_{\omega \in \mathbb{F}_z} \frac{|\bar{f}_{B+k+1}(\omega) - \bar{f}_{B+k+1}(\omega)|}{S_{B+k}(\omega)} < \varepsilon,$$

where $S(\omega)$ is the asymptotic standard deviation of the complete data smoothed periodogram

$$S_{B+k}(\omega) = \left(\sum_{\nu \in \mathbb{F}_z} \bar{f}_{B+k}(\nu)^2 \alpha(\omega - \nu)^2 \right)^{1/2}.$$

We have found that $\varepsilon = 0.05$ is a reasonable convergence tolerance criterion, and we choose $B = 30$ burn-in iterations. We use a cross-validation procedure to choose the smoothing

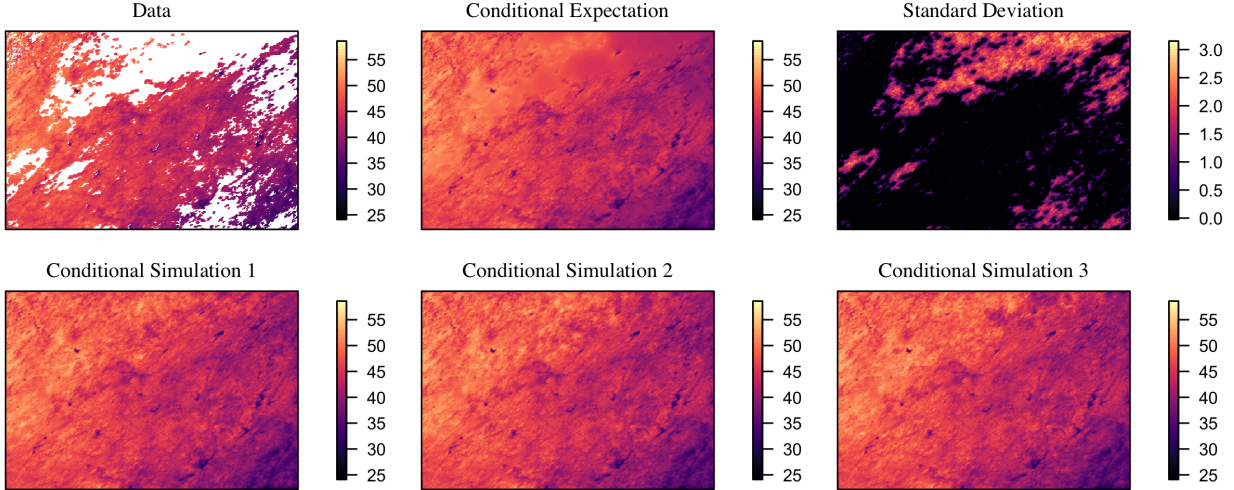


Figure 6: Original data, predictions, standard deviations, and three conditional simulations of the missing values

parameter. A random subset of 30% of the data is held out, and the iterative methods are run with a range of smoothing parameters, and the parameter that minimizes sum of squared prediction errors is chosen.

In Figure 6, we plot the original data, the conditional expectation, an estimate of the conditional standard deviations, and three conditional simulation plots. The conditional standard deviations are estimated by computing 30 conditional simulations, and computing the root mean squared difference between the conditional expectation and each of the conditional simulations at each pixel. Conditional simulations are a useful tool for propagating uncertainty of predictions through a broader analysis; for example, if land surface temperature is an input to a numerical pollution model, the pollution model can be run several times with an ensemble of conditionally simulated land surface temperature datasets in order to investigate the uncertainty introduced by predicting missing values. On average, the conditional simulations took just 2.76 seconds and converged in 25 iterations with the Vecchia preconditioner, and took 15.48 seconds and converged in 159 iterations with the inverse spectrum preconditioner. The iterative spectrum estimation method took 4.86 minutes to converge. All timings are done on a 2016 Macbook Pro with 3.3 GHz Intel Core i7 processor (dual core) and with 16GB Memory, running R 3.4.2 linked to Apple’s Accelerate BLAS libraries. Reported time is elapsed time from calls to `proc.time`.

Visually, the data appear to have a longer correlation lengthscale in the northeast-southwest direction than in the southeast-northwest direction. The estimate of the spectrum returned by the iterative method confirms our visual suspicions, as can be seen in Figure 7, where the logarithm of the estimated spectrum is plotted. The estimated spectrum shows clear signs of anisotropy in that the spectrum has contours that are not circular. In general, it has been our experience that anisotropic parametric models are difficult to fit via maximum likelihood, due to the large number of parameters (typically 5 or 6 with the Matérn covariance: variance, smoothness, two range parameters, anisotropy angle, and nugget), and due to periodicities in the parameter space. In contrast, the nonparametric spectral density

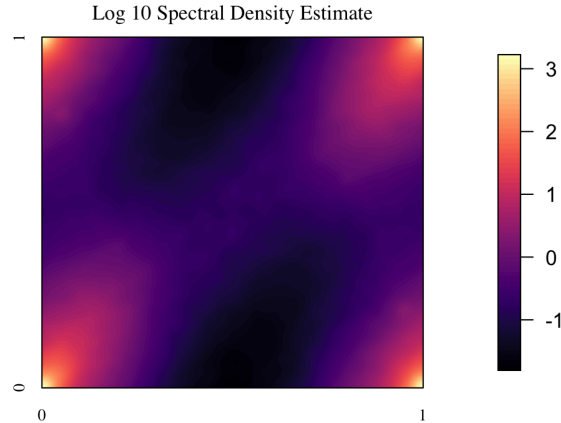


Figure 7: Log base 10 of spectral density estimate.

estimation methods automatically estimated the anisotropies with no extra effort.

6 Discussion

This paper introduces improved methods for estimating spectral densities of random fields on d -dimensional lattices from incomplete observations. Given an estimate of the spectrum, data are conditionally simulated on an expanded lattice according to a periodic model derived from the spectrum. Then the spectrum estimate is updated using the imputed data, and the procedure is iterated until convergence. In addition, we introduce a parametric filtering method that, due to the imputation step, can be implemented even when there are a substantial number of missing values. We provide several theoretical results that consider the rate of decay of the error in the bispectrum, which is informative about periodogram bias and about correlation in the discrete Fourier transform vector. The methods are demonstrated in numerical and simulation studies and in an application to interpolation of land surface temperature data. Periodic imputations are shown to have a remarkable ability to give highly accurate and unbiased estimates of the spectral density, especially when combined with the parametric filtering method.

The methods involve choosing the factor by which the lattice should be expanded. We have found that even very small factors that expand the lattice by a few pixels are effective at improving the spectral density estimates. We recommend expanding each dimension by an amount roughly equal to the correlation range in the data. As with most nonparametric spectral density estimates, the methods involve the choice of a smoothing parameter. We have not attempted to provide any new methods for selecting smoothing parameters, as this issue has been well-studied in the literature. However, we note that the parametric filtering methods serve to flatten the periodogram, which makes the estimates less sensitive to the choice of smoothing parameter. In our application to land surface temperature data, we used a cross-validation procedure to select the smoothing parameter.

While many large datasets involve spatially gridded observations, we acknowledge that there is also a need for methods for analyzing non-gridded data. The nonparametric meth-

ods described in this paper may prove useful for analyzing non-gridded data as well; in fact Nychka et al. (2015) have a framework for analyzing non-gridded data that includes lattice process with a Markov assumption as a model component. We have considered stationary models here. Stationary models can be used as components in nonstationary models (Fuentes, 2002), and so the methods developed here could potentially be extended to be used for local nonparametric estimation of nonstationary models as well.

Acknowledgements

This material is based upon work supported by the National Science Foundation under Grant No. 1613219.

A Proofs of Theorems

Theorem 1. *If $f_1 = f$, $K(h) = 0$ for all $\|h\| > h_0$, and $|z_j - y_j| > h_0$ for all $j \in \{1, \dots, d\}$, then for every $\nu, \omega \in \mathbb{F}_z$,*

$$\tilde{f}(\nu, \omega) - f(\nu, \omega) = 0.$$

Proof. We have $f(\nu, \omega) = g(\nu)^\dagger R g(\omega)$, and so $\tilde{f}(\nu, \omega) - f(\nu, \omega) = g(\nu)^\dagger (S - R) g(\omega)$. The matrix $S - R$ can be written as

$$S - R = \begin{bmatrix} K - A & (K - A)A^{-1}B \\ B^T A^{-1}(K - A) & B^T A^{-1}(K - A)A^{-1}B \end{bmatrix}.$$

It suffices to show that $K = A$ in order to establish the result. According to the multidimensional Poisson summation formula, we can relate $K(\cdot)$ and $R(\cdot)$ as

$$R(x_1 - x_2) = \sum_{k \in \mathbb{Z}^d} K(x_1 - x_2 + (z \circ k)) = K(x_1 - x_2) + \sum_{k \in \mathbb{Z}^d \setminus 0} K(x_1 - x_2 + (z \circ k)), \quad (5)$$

where $z \circ k := (z_1 k_1, \dots, z_d k_d)$. For any $x_1, x_2 \in \mathbb{J}_y$ (the observation lattice), we have $|x_{1j} - x_{2j}| < y_j$ for every $j = 1, \dots, d$. Thus if $k_j \in \mathbb{Z} \setminus 0$, $|x_{1j} - x_{2j} + z_j k_j| > |z_j - y_j| > h_0$. Thus at least one element of $x_1 - x_2 + (z \circ k)$ has absolute value greater than h_0 when $k \in \mathbb{Z}^d \setminus 0$, and so $\|x_1 - x_2 + (z \circ k)\| > h_0$ for all $k \in \mathbb{Z}^d \setminus 0$, implying that all terms in the sum in (5) must be zero. This gives us $R(x_1 - x_2) = K(x_1 - x_2)$ for any $x_1, x_2 \in \mathbb{J}_y$, and so $K = A$. \square

Theorem 2. *If f has p continuous partial derivatives, $f_1 = f$, $y_j = O(n^{1/d})$, and $z_j = O(\tau y_j)$ for $\tau > 1$, then for every $\nu, \omega \in \mathbb{F}_z$,*

$$\tilde{f}_1(\nu, \omega) - f(\nu, \omega) = O(n^{-p/d+1}).$$

Proof. As in the proof of Theorem 1, $\tilde{f}(\nu, \omega) - f(\nu, \omega) = g(\nu)^\dagger (S - R)g(\omega)$. Partitioning the vector $g(\nu)$ as $(g_1(\nu), g_2(\nu))$ according to the same partition as (U, V) , we have

$$\begin{aligned}\tilde{f}(\nu, \omega) - f(\nu, \omega) &= [g_1(\nu)^\dagger \ g_2(\nu)^\dagger] \begin{bmatrix} K - A & (K - A)A^{-1}B \\ B^T A^{-1}(K - A) & B^T A^{-1}(K - A)A^{-1}B \end{bmatrix} \begin{bmatrix} g_1(\omega) \\ g_2(\omega)^\dagger \end{bmatrix} \\ &= (g_1(\nu)^\dagger + g_2(\nu)^\dagger B^T A^{-1})(K - A)(g_1(\omega) + A^{-1}B g_2(\omega)),\end{aligned}$$

and so the difference can be bounded as

$$\begin{aligned}|\tilde{f}(\nu, \omega) - f(\nu, \omega)| &= |(g_1(\nu)^\dagger + g_2(\nu)^\dagger B^T A^{-1})(K - A)(g_1(\omega) + A^{-1}B g_2(\omega))| \\ &\leq \|g_1(\nu) + A^{-1}B g_2(\nu)\|_2 \|K - A\|_2 \|g_1(\omega) + A^{-1}B g_2(\omega)\|_2.\end{aligned}$$

We will consider each term in turn. Let $\rho(M)$ denote the spectral radius of symmetric matrix M . Then

$$\begin{aligned}\|g_1(\nu) + A^{-1}B g_2(\nu)\|_2 &\leq \|g_1(\nu)\|_2 + \|A^{-1}B g_2(\nu)\|_2 \\ &\leq \sqrt{\frac{n}{m}} + \|A^{-1/2}\|_2 \|A^{-1/2}B\|_2 \|g_2(\nu)\|_2 \\ &= \sqrt{\frac{n}{m}} + \rho(A^{-1})^{1/2} \rho(B^T A^{-1}B)^{1/2} \|g_2(\nu)\|_2 \\ &\leq \sqrt{\frac{n}{m}} + f_{\min}^{-1/2} \rho(C)^{1/2} \sqrt{\frac{m-n}{m}} \\ &\leq \sqrt{\frac{n}{m}} + \sqrt{\frac{f_{\max}}{f_{\min}}} \sqrt{\frac{m-n}{m}},\end{aligned}$$

where in the second to last inequality, we used $\rho(A^{-1}) < \rho(R^{-1}) = f_{\min}^{-1}$, and $C - B^T A^{-1}B$ positive definite, so the largest eigenvalue of $B^T A^{-1}B$ is smaller than the largest eigenvalue of C , which is smaller than the largest eigenvalue of R , f_{\max} .

The previous inequality did not depend on ν , so it holds for $\|g_1(\omega) + A^{-1}B g_2(\omega)\|_2$ as well. To bound $\|K - A\|_2$, we use the fact that for symmetric matrices $\|K - A\|_2 = \rho(K - A) < \|K - A\|_1$, where

$$\begin{aligned}\|K - A\|_1 &= \max_i \sum_{j=1}^n |K_{ij} - A_{ij}| \\ &= \max_{x_1 \in \mathbb{J}_y} \sum_{x_2 \in \mathbb{J}_y} \left| \sum_{k \neq \mathbf{0}} K(x_1 - x_2 + (k \circ z)) \right| \\ &\leq \max_{x_1 \in \mathbb{J}_y} \sum_{x_2 \in \mathbb{J}_y} \sum_{k \neq \mathbf{0}} \left| K(x_1 - x_2 + (k \circ z)) \right|\end{aligned}$$

The second equality uses the multidimensional Poisson summation formula. By assumption, for $k = (k_1, \dots, k_d) \neq \mathbf{0}$ and any $x_1, x_2 \in \mathbb{J}_y$,

$$\max_{1 \leq j \leq d} |x_{1j} - x_{2j} + z_j k_j| \geq \min_{1 \leq j \leq d} |z_j - y_j|.$$

This is because $k_j \neq 0$ for at least one j . Define $\ell_{\min} = \min_{1 \leq j \leq d} |z_j - y_j|$, which is the embedding distance in the dimension with the smallest amount of embedding. By assumption, we have

$$\ell_{\min} > \min_{1 \leq j \leq d} \lfloor (\tau - 1)y_j \rfloor > \min_{1 \leq j \leq d} \lfloor (\tau - 1)a_j n^{1/d} \rfloor.$$

This means the sum does not contain any terms $K(h)$ for which $\max_j |h_j| < \ell_{\min}$. Define the set $G_\ell = \{h : \max_j |h_j| = \ell\}$, which is a hollowed out cube on \mathbb{Z}^d and has size $|G_\ell| = (2\ell + 1)^d - (2\ell - 1)^d = O(\ell^{d-1})$. Using this notation, the sum can be bounded as

$$\|K - A\|_1 \leq \sum_{\ell=\ell_{\min}}^{\infty} \sum_{h \in G_\ell} |K(h)|.$$

Lemma 9.5 in Körner (1989) states that if f has p continuous partial derivatives on \mathbb{T}^d , with maximum p th partial derivative $Q_p(f)$, then

$$|K(h)| \leq Q_p(f)|h_j|^{-p}$$

for every $1 \leq j \leq d$, and so we can use the bound $|K(h)| \leq Q_p(f)(\max_{1 \leq j \leq d} |h_j|)^{-p}$. This gives us an explicit bound

$$\begin{aligned} \|K - A\|_1 &\leq \sum_{\ell=\ell_{\min}}^{\infty} \sum_{h \in G_\ell} \frac{Q_p(f)}{\ell^p} = \sum_{\ell=\ell_{\min}}^{\infty} \left((2\ell + 1)^d - (2\ell - 1)^d \right) \frac{Q_p(f)}{\ell^p} \\ &= \sum_{\ell=\ell_{\min}}^{\infty} Q_p(f) \frac{a_{d-1}(\ell)}{\ell^p}, \end{aligned}$$

where $a_{d-1}(\ell)$ is a polynomial of degree $d - 1$ in ℓ . Then we have

$$\|K - A\|_1 = O(\ell_{\min}^{-p+d}) = O(n^{-p/d+1})$$

since the largest exponent in $a_{d-1}(\ell)/\ell^p$ is $-p + d - 1$. Combining this with $\|g_1(\nu) + A^{-1}Bg_2(\nu)\| = O(1)$ gives the desired result. \square

Theorem 3. *Let f have p continuous partial derivatives, and assume the same conditions on the observation and embedding lattice as in Theorem 2. Define $\Delta_1 = \max_{\omega \in [0,1]^d} |f(\omega) - f_1(\omega)|$. Then for every $\nu, \omega \in \mathbb{F}_z$,*

$$\tilde{f}_1(\nu, \omega) - f(\nu, \omega) = O(n^{-p/d+1}) + O\left(\Delta_1 \sqrt{\frac{m-n}{m}}\right),$$

meaning that the difference contains two terms with the respective rates.

Proof. Define the matrix S_1 as

$$S_1 = \begin{bmatrix} A & AA_1^{-1}B_1 \\ B_1^T A_1^{-1}A & C_1 - B_1^T A_1^{-1}B_1 + B_1^T A_1^{-1}AA_1^{-1}B_1 \end{bmatrix},$$

which differs from S in that K in S is replaced by A in S_1 . The difference $\tilde{f}_1(\nu, \omega) - f(\nu, \omega)$ can be written as

$$g(\nu)^\dagger (S - R)g(\omega) = g(\nu)^\dagger (S - S_1)g(\omega) + g(\nu)^\dagger (S_1 - R_1 + R_1 - R)g(\omega). \quad (6)$$

The first term in (6) is

$$\begin{aligned} \delta_1 &:= \begin{bmatrix} g_1(\nu)^\dagger & g_2(\nu)^\dagger \end{bmatrix} \begin{bmatrix} K - A & (K - A)A_1^{-1}B_1 \\ B_1^T A_1^{-1}(K - A) & B_1^T A_1^{-1}(K - A)A_1^{-1}B_1 \end{bmatrix} \begin{bmatrix} g_1(\omega) \\ g_2(\omega)^\dagger \end{bmatrix} \\ &= (g_1(\nu)^\dagger + g_2(\nu)^\dagger B_1^T A_1^{-1})(K - A)(g_1(\omega) + A_1^{-1}B_1 g_2(\omega)). \end{aligned}$$

This expression has a similar form to that which appears in the proof of Theorem 2. As before, we need bounds for $\|g_1(\omega) + A_1^{-1}B_1 g_2(\omega)\|_2$ and $\|K - A\|_2$ in order to bound δ_1 . The proof for the bound on $\|K - A\|_2$ is identical to that in Theorem 2, and the proof for the bound on $\|g_1(\omega) + A_1^{-1}B_1 g_2(\omega)\|_2$ is similar, although f is replaced by f_1 , which does not change the overall result that the first term in (6) is $O(n^{-p/d+1})$.

To shorten the equations to follow, write $M_1 = A_1^{-1}B_1$. The second term in (6) is

$$\begin{aligned} \delta_2 &:= \begin{bmatrix} g_1(\nu)^\dagger & g_2(\nu)^\dagger \end{bmatrix} \begin{bmatrix} A - A_1 & (A - A_1)M_1 \\ M_1^T(A - A_1) & M_1^T(A - A_1)M_1 \end{bmatrix} \begin{bmatrix} g_1(\omega) \\ g_2(\omega)^\dagger \end{bmatrix} + f_1(\nu, \omega) - f(\nu, \omega) \\ &= (g_1(\nu)^\dagger + g_2(\nu)^\dagger M_1^T)(A - A_1)(g_1(\omega) + M_1 g_2(\omega)) + f_1(\nu, \omega) - f(\nu, \omega). \end{aligned}$$

Partition the DFT matrix F into rows for the observations and missing values as $F^\dagger = [G^\dagger H^\dagger]$. We have $R = FDF^\dagger$, where D is diagonal with entries $f(\nu, \omega)$. This gives $A = GDG^\dagger$, and likewise $A_1 = GD_1G^\dagger$, where D_1 is diagonal with entries $f_1(\nu, \omega)$. Then δ_2 can then be written as

$$\delta_2 = (g_1(\nu)^\dagger G + g_2(\nu)^\dagger M_1^T G)(D - D_1)(G^\dagger g_1(\omega) + G^\dagger M_1 g_2(\omega)) + f_1(\nu, \omega) - f(\nu, \omega).$$

Note that $I = G^\dagger G + H^\dagger H$. Since $g_1(\nu)^\dagger$ is a row of G^\dagger , and $g_2(\nu)^\dagger$ is the same row of H^\dagger we have

$$g_1(\nu)^\dagger G + g_2(\nu)^\dagger H = e(\nu),$$

where $e(\nu) = 1$ for the entry corresponding to ν and 0 otherwise. This gives

$$\delta_2 = (e(\nu)^T + g_2(\nu)^\dagger (M_1^T G - H))(D - D_1)(e(\omega) + (G^\dagger M_1 - H^\dagger)g_2(\omega)) + f_1(\nu, \omega) - f(\nu, \omega).$$

We can see now that since $e(\nu)^T (D - D_1) e(\omega) = f(\nu, \omega) - f_1(\nu, \omega)$, there is a cancellation, giving

$$\begin{aligned} \delta_2 &= g_2(\nu)^\dagger (M_1^T G - H)(D - D_1)e(\omega) + e(\nu)^T (D - D_1)(G_1^\dagger M_1 - H^\dagger)g_2(\omega) \\ &\quad + g_2(\nu)^\dagger (M_1^T G - H)(D - D_1)(G_1^\dagger M_1 - H^\dagger)g_2(\omega). \end{aligned}$$

This cancellation is the key step. Using matrix norm inequalities, we have

$$\begin{aligned} |\delta_2| &\leq \|g_2(\nu)\|_2 \|M_1^T G - H\|_2 \|D - D_1\|_2 \|e(\omega)\|_2 \\ &\quad + \|g_2(\omega)\|_2 \|M_1^T G - H\|_2 \|D - D_1\|_2 \|e(\nu)\|_2 \\ &\quad + \|g_2(\omega)\|_2 \|g_2(\nu)\| \|M_1^T G - H\|_2^2 \|D - D_1\|_2 \|e(\nu)\|_2 \end{aligned}$$

Since $g_2(\omega)$ is of length n_2 and has entries $n^{-1/2} \exp(2\pi i \omega \cdot x)$, $\|g_2(\omega)\|_2 = \sqrt{n_2/n}$. Clearly, $\|e(\omega)\| = 1$ because of its definition, and $\|D - D_1\|_2 = \Delta_1$ because both D and D_1 are diagonal with diagonal entries holding $f(\nu, \nu)$ and $f_1(\nu, \nu)$, respectively. This leaves

$$\|M_1^T G - H\|_2^2 = \rho(M_1^T G - H)(G^\dagger M_1 - H^\dagger) = \rho(M_1^T M_1 + I),$$

because $GG^\dagger = I$, $HH^\dagger = I$, $HG^\dagger = 0$, and $GH^\dagger = 0$. Thus, the squared 2-norm is 1 plus the largest eigenvalue of $M_1^T M_1$, which is

$$\|M_1^T M_1\|_2 = \|M_1\|_2^2 = \|A_1^{-1} B_1\|_2^2 \leq \frac{f_{1,\max}}{f_{1,\min}},$$

with the last inequality following from the proof of Theorem 2. Bringing this all together gives

$$\begin{aligned} |\delta_2| &\leq 2\sqrt{\frac{m-n}{m}}\sqrt{1 + \frac{f_{1,\max}}{f_{1,\min}}}\Delta_1 + \frac{m-n}{m}\left(1 + \frac{f_{1,\max}}{f_{1,\min}}\right)\Delta_1 \\ &= O\left(\sqrt{\frac{m-n}{m}}\Delta_1\right), \end{aligned}$$

establishing the second term of the Theorem. □

References

Chiles, J.-P. and Delfiner, P. (2009). *Geostatistics: Modeling Spatial Uncertainty*, volume 497. John Wiley & Sons.

Chow, Y.-S. and Grenander, U. (1985). A sieve method for the spectral density. *The Annals of Statistics*, pages 998–1010.

Dahlhaus, R. and Künsch, H. (1987). Edge effects and efficient parameter estimation for stationary random fields. *Biometrika*, 74(4):877–882.

Fuentes, M. (2002). Spectral methods for nonstationary spatial processes. *Biometrika*, 89(1):197–210.

Fuentes, M. (2007). Approximate likelihood for large irregularly spaced spatial data. *Journal of the American Statistical Association*, 102(477):321–331.

Greenbaum, A. (1997). *Iterative methods for solving linear systems*. SIAM.

Guinness, J. and Fuentes, M. (2017). Circulant embedding of approximate covariances for inference from Gaussian data on large lattices. *Journal of Computational and Graphical Statistics*, 26(1).

Guyon, X. (1982). Parameter estimation for a stationary process on a d-dimensional lattice. *Biometrika*, 69(1):95–105.

Heaton, M. J., Datta, A., Finley, A., Furrer, R., Guhaniyogi, R., Gerber, F., Gramacy, R. B., Hammerling, D., Katzfuss, M., and Lindgren, F. (2017). Methods for analyzing large spatial data: A review and comparison. *arXiv preprint arXiv:1710.05013*.

Heyde, C. and Gay, R. (1993). Smoothed periodogram asymptotics and estimation for processes and fields with possible long-range dependence. *Stochastic Processes and their Applications*, 45(1):169–182.

Körner, T. W. (1989). *Fourier Analysis*. Cambridge University Press.

Lee, T. C. (1997). A simple span selector for periodogram smoothing. *Biometrika*, 84(4):965–969.

Lee, T. C. (2001). A stabilized bandwidth selection method for kernel smoothing of the periodogram. *Signal Processing*, 81(2):419–430.

Lee, T. C. and Zhu, Z. (2009). Nonparametric spectral density estimation with missing observations. In *Acoustics, Speech and Signal Processing, 2009. ICASSP 2009. IEEE International Conference on*, pages 3041–3044. IEEE.

Lim, C. Y. and Stein, M. (2008). Properties of spatial cross-periodograms using fixed-domain asymptotics. *Journal of Multivariate Analysis*, 99(9):1962–1984.

Lindgren, F., Rue, H., and Lindström, J. (2011). An explicit link between Gaussian fields and Gaussian Markov random fields: the stochastic partial differential equation approach. *Journal of the Royal Statistical Society: Series B (Statistical Methodology)*, 73(4):423–498.

Nychka, D., Bandyopadhyay, S., Hammerling, D., Lindgren, F., and Sain, S. (2015). A multiresolution Gaussian process model for the analysis of large spatial datasets. *Journal of Computational and Graphical Statistics*, 24(2):579–599.

Ombao, H. C., Raz, J. A., Strawderman, R. L., and Von Sachs, R. (2001). A simple generalised crossvalidation method of span selection for periodogram smoothing. *Biometrika*, 88(4):1186–1192.

Pawitan, Y. and O’Sullivan, F. (1994). Nonparametric spectral density estimation using penalized Whittle likelihood. *Journal of the American Statistical Association*, 89(426):600–610.

Politis, D. N. and Romano, J. P. (1995). Bias-corrected nonparametric spectral estimation. *Journal of Time Series Analysis*, 16(1):67–103.

Stein, M. L. (1995). Fixed-domain asymptotics for spatial periodograms. *Journal of the American Statistical Association*, 90(432):1277–1288.

Stroud, J. R., Stein, M. L., and Lysen, S. (2017). Bayesian and maximum likelihood estimation for Gaussian processes on an incomplete lattice. *Journal of Computational and Graphical Statistics*, 26(1):108–120.

Sykulski, A. M., Olhede, S. C., and Lilly, J. M. (2016). The de-biased Whittle likelihood for second-order stationary stochastic processes. *arXiv preprint arXiv:1605.06718*.

Tanner, M. A. and Wong, W. H. (1987). The calculation of posterior distributions by data augmentation. *Journal of the American Statistical Association*, 82(398):528–540.

Vecchia, A. V. (1988). Estimation and model identification for continuous spatial processes. *Journal of the Royal Statistical Society. Series B (Methodological)*, 50(2):297–312.

Wahba, G. (1980). Automatic smoothing of the log periodogram. *Journal of the American Statistical Association*, 75(369):122–132.

Whittle, P. (1954). On stationary processes in the plane. *Biometrika*, 41(3/4):434–449.

Wood, A. T. and Chan, G. (1994). Simulation of stationary Gaussian processes in $[0, 1]^d$. *Journal of Computational and Graphical Statistics*, 3(4):409–432.

Zheng, Y., Zhu, J., and Roy, A. (2009). Nonparametric Bayesian inference for the spectral density function of a random field. *Biometrika*, 97(1):238–245.